ORIGINAL RESEARCH

Changes in Fiber Integrity, Diffusivity, and Metabolism of the Pyramidal Tract Adjacent to Gliomas: A Quantitative Diffusion Tensor Fiber Tracking and MR Spectroscopic Imaging Study

A. Stadlbauer
C. Nimsky
S. Gruber
E. Moser
T. Hammen
T. Engelhorn
M. Buchfelder
O. Ganslandt

BACKGROUND AND PURPOSE: The underlying changes in the neuronal connectivity adjacent to brain tumors cannot always be depicted by conventional MR imaging. The hypothesis of this study was that preoperative sensorimotor deficits are associated with impairment in pyramidal fiber bundles. Hence, we investigated the potential of combined quantitative diffusion tensor (DT) fiber tracking and MR spectroscopic imaging (MRSI) to determine changes in the pyramidal tract adjacent to gliomas.

MATERIALS AND METHODS: Quantitative DT fiber tracking and proton MRSI were performed in 20 patients with gliomas with WHO grades II–IV. Eight patients experienced preoperative sensorimotor deficits. Mean diffusivity (MD), fractional anisotropy (FA), and number of fibers per voxel (FpV) were calculated for the pyramidal tract of the ipsilateral and contralateral hemisphere. Metabolite concentrations for choline-containing compounds (Cho), creatine (Cr), and *N*-acetylaspartate (NAA) were computed, using LCModel, for all voxels located at the pyramidal tracts.

RESULTS: For the whole pyramidal tract, quantitative DT fiber tracking resulted in significantly lower FpV and FA values ($P < .001$), but not MD values, for the ipsilateral hemisphere. For the section of the fiber bundle closest to the lesion, we found significantly decreased FpV and FA ($P < .001$) and increased MD ($P = .002$). MRSI showed, for the same volumes of interest, significantly decreased NAA ($P = .001$), increased Cho ($P = .034$) and Cho/NAA ($P = .001$) for the ipsilateral pyramidal tract. In patients suffering sensorimotor deficits, we found significantly lower FA ($P = .022$) and higher MD values ($P = .026$) and a strongly negative correlation between FA and MD ($R = -0.710$, $P = .024$) but no correlation in patients without deficits ($R = 0.078$, ns).

CONCLUSION: Quantitative DTI was able to show significant differences in diffusivity of the pyramidal tract in patients with sensorimotor deficits in relation to patients without them. The additional use of proton MRSI may be helpful to discern whether these diffusivity changes in fiber tracts are caused by tumor infiltration or peritumoral edema.

The pyramidal tract is a major pathway of the central nervous system. This massive collection of axons originates from the motor cortex areas and the postcentral gyrus and descends through the brain stem to the spinal cord. Mild impairment or even damage of the corticospinal fibers is often seen in patients with glioma and may result in sensorimotor deficits. Conventional MR imaging, however, cannot always depict the underlying changes of the affected fiber bundles.

MR diffusion tensor imaging (DTI) enables detection of anisotropic water diffusion in the brain[1,2] using at least 6 different diffusion gradient directions. The anisotropy of water diffusion in the white matter (WM) derives from its organization in myelinated axonal fibers, where diffusion is slowest perpendicular to the fiber tract.[3] It is common practice to calculate parametric maps of mean diffusivity (MD) and fractional anisotropy (FA) out of DTI data combined with manual segmentation of regions of interest (ROIs) for evaluation. MD and FA describe the magnitude and directionality of water diffusion, respectively. Fiber tracking is another method for evaluating DTI data that permits in vivo investigation of neuronal fibers using a tracking algorithm that compares the information about the orientation of water diffusion on a voxel-to-voxel basis. Recent studies have shown possibility to reconstruct fiber tracts adjacent to the tumor even if the tracts are displaced, disrupted, or invaded by the tumor.[4-7] The reconstructed fiber bundles are commonly used for visual or qualitative assessment. Quantitative fiber tracking[8-10] is an approach to determine DTI (eg, FA and MD) and fiber parameters (eg, fiber attenuation) of WM structures using a fiber-tracking algorithm for semiautomatic segmentation of the volumes of interest in the brain.

Proton MR spectroscopic imaging (^{1}H-MRSI) allows the noninvasive investigation of the spatial distribution of metabolic changes in and around brain lesions. Although no tumor-specific metabolites can be measured using in vivo MRSI, it is possible, however, to detect specific patterns in changes of metabolite concentrations compared with the normal brain. It is well known that gliomas show increased levels of choline-containing compounds (Cho) and a reduction in the signal intensity of the *N*-acetylaspartate (NAA).[11,12] Cho is thought to be a marker for increased membrane turnover or higher cellular attenuation.[13] NAA is identified as neuronal marker mainly contained within neurons.[14]

It was the purpose of our study, using quantitative fiber tracking and proton MR spectroscopic imaging with high spa-

Received April 5, 2006; accepted after revision May 23.

From the Departments of Neurosurgery (A.S., C.N., M.B., O.G.), Neurology (T.H.), and Neuroradiology (T.E.), University of Erlangen-Nuremberg, Germany; and MR Center of Excellence (S.G., E.M.) and Department of Diagnostic-Radiology (S.G., E.M.), Medical University of Vienna, Austria.

This study was supported by the German Research Society Grants SFB 603, C9, and DFG GA 638/2-1.

Address correspondence to Oliver Ganslandt, MD, Schwabachanlage 6, 91054 Erlangen, Germany; e-mail: ganslandt@nch.imed.uni-erlangen.de

Table 1: Type, grade, and location of the investigated brain tumors and preoperative sensorimotor deficits of the 20 patients

Patient	Age (Years)	Sex	Clinical Diagnosis and Lesion Location	Lesion Location Relative to PT	Preoperative Sensorimotor Deficits
1	29	M	Oligoastrocytoma III, right frontal	Medial	Paresthesia, left arm and leg
2	24	M	Astrocytoma II, right frontal	Lateral	None
3	35	F	Oligodendroglioma III, left frontal	Anterior	Paresthesia, right leg
4	29	F	Astrocytoma II, right central	Anterior	None
5	39	F	Oligoastrocytoma III, left frontal	Anterior	Hemiparesis, right
6	29	M	Astrocytoma III, right frontal	Anterior	None
7	64	M	GBM IV, right temporoparietal	Posterior	Hemiparesis, hemihypesthesia, left
8	29	M	Oligoastrocytoma III, left temporal	Lateral	None
9	37	M	Astrocytoma II, right frontotemporal	Anterior	None
10	30	M	Astrocytoma III, right temporal	Anterior	None
11	53	F	Oligoastrocytoma II, left central	Anterior	None
12	30	M	Astrocytoma II, right postcentral	Lateral	Hypesthesia, left arm and leg
13	42	F	Astrocytoma III, left central	Medial	None
14	29	M	Astrocytoma II, left postcentral	Lateral	Hypesthesia, right arm
15	37	F	Oligoastrocytoma III, right frontal	Lateral	None
16	39	F	GBM IV, left frontal	Medial	None
17	63	M	Astrocytoma III, left postcentral	Lateral	None
18	72	F	GBM IV, left frontal	Anterior	Hemiparesis, hemihypesthesia, right
19	52	M	Oligoastrocytoma III, right frontal	Anterior	None
20	50	F	GBM IV, right temporal	Lateral	Hemiparesis, left

Note:—M indicates male; F, female; GBM, glioblastoma multiforme; PT, pyramidal tract.

tial resolution, to assess changes in fiber integrity, diffusivity, and brain metabolism of the pyramidal tract adjacent to WHO grade II, III, and IV gliomas compared with the contralateral normal-appearing brain. The combination of DT fiber tracking and MRSI was performed to discriminate between tumor infiltration and peritumoral edema. These conditions change the fiber integrity and diffusivity. The metabolic changes had to be assessed noninvasively by MRSI because it is not possible to obtain biopsies out of the pyramidal tract. We hypothesized that preoperative sensorimotor deficits are associated with impairment in fiber bundles of the pyramidal tract adjacent to the tumor. Therefore, an additional objective was to determine differences in the pyramidal tract between patients with and without preoperative sensorimotor deficits.

Materials and Methods

Patients

We examined 20 patients (age range, 24–72 years; mean age ± SD, 40.6 ± 13.9 years) with untreated supratentorial gliomas of WHO grades II, III, or IV before surgery. Nine patients were female, and 8 patients experienced paresis, paresthesia, and/or hypesthesia before surgery. Information about the type and location of the tumors and the sensorimotor deficits is summarized in Table 1. For this retrospective study, the ethics committee of the University Erlangen-Nuremberg did not require its approval or informed consent. However, signed informed consent was obtained from all patients for imaging procedures performed.

MR Data Acquisition

MR examinations, including conventional MR imaging, DTI, and ^{1}H-MRSI, were performed on a 1.5T clinical whole-body scanner (Magnetom Sonata; Siemens, Erlangen, Germany) equipped with the standard head coil. Conventional MR imaging consisted of 1) an axial turbo spin-echo (TSE) sequence (TR, 5600–6490 ms; TE, 98 ms; section thickness, 5 mm), 2) an axial fluid-attenuated inversion recovery (FLAIR) sequence (TR, 10,000; TE, 103 ms; section thickness, 5 mm), 3) an axial spin-echo (SE) sequence (T1-weighted, TR, 500 ms; TE, 15 ms; matrix size, 256 × 256; FOV, 16 × 16 cm; 20 sections with no gap; section thickness, 2 mm) that was used for integration of spectroscopic data into the planning station of a stereotactic system,[15] and 4) pregadolinium and postgadolinium contrast-enhanced 3D magnetization-prepared rapid acquisition of gradient echo (MPRAGE) sequences (TR, 2020; TE 4.38 ms; isotropic matrix, 1 mm; FOV, 250 × 250 mm; 160 sections).

For DTI, a diffusion-weighted echo-planar imaging (EPI) sequence was used with the following parameters: TR, 9200; TE, 86 ms; matrix size, 128 × 128; FOV, 240 × 240 mm; section thickness, 1.9 mm; bandwidth, 1502 Hz/pixel. Sixty axial sections were measured with no intersectional gap and an isotropic voxel size of 1.9 × 1.9 × 1.9 mm^3. Diffusion gradient encoding in 6 directions with $b = 1000$ s/mm^2 and an additional measurement without diffusion gradient ($b = 0$ s/mm^2) were performed. The sequence design was based on balanced diffusion gradients to minimize eddy-current artifacts. For sufficient signal-to-noise ratio (SNR), 5 averages were applied, requiring a total DTI data acquisition time of 5 minutes 31 seconds

The MRSI examination immediately followed the DTI. The volume of interest (VOI) of the MRSI experiment with point-resolved spectroscopy sequence (PRESS) volume preselection, a so-called PRESS-box, was aligned parallel to those of the axial T2-weighted TSE and T1-weighted SE sections that showed the maximal dimension of the lesion. Furthermore, the PRESS box was positioned to exclude lipids of the skull and subcutaneous fat. MRSI parameters chosen were TR, 1600 ms; TE, 135 ms; 24 × 24 circular phase encoding scheme across a 16 × 16-cm FOV; section thickness, 10 mm; 50%

Hamming filter; NEX, 2; spectral width, 1000 Hz; acquisition size, 1024 complex points. The total spectroscopic data acquisition time was less than 13 minutes. Immobilization of the patient's head to minimize artifacts due to patient motion was achieved by fixation in a headrest.

MR Data Analysis

DTI data were transferred to a workstation (Inspiron 8200; Dell Computer Co, Round Rock, Tex) for analysis. Data processing was performed using DTIStudio (version 2.4; Johns Hopkins University, Baltimore, Md).[16] Three eigenvalues (λ_1, λ_2, λ_3) and 3 eigenvectors, as well as parametric maps of FA and MD, were calculated.[17]

Fiber tracking was performed by designating ROIs to define areas of the precentral and postcentral gyrus as seed areas (mean ROI area ± SD = 1120 ± 205 mm^2). To serve as target areas, ROIs were placed to encompass the entire posterior limb of the internal capsule (mean ROI area ± SD = 216 ± 34 mm^2). For 3D reconstruction of pyramidal tracts, the fiber assignment by continuous tracking method was used.[1,18] The tracking procedure was stopped when a track turning angle greater than 60° was encountered. A lower threshold of FA = 0.15, which was found to be optimal for the appliance of fiber tracking procedures in glioma patients,[19] was used as the indicator for termination of tract elongation. The tracking procedure was terminated at a pixel with an FA value lower than the threshold. Quantitative fiber tracking of the reconstructed fibers was performed using the "tract statistics" function of DTIStudio, which enables the statistical evaluation of parameters of voxels occupied by reconstructed fibers. The calculated DTI and fiber parameters for the pyramidal tracts were FA, MD, and mean number of fibers per voxel (FpV), which can be interpreted as a measure for the fiber attenuation of the selected fiber bundle.

MRSI data were evaluated to obtain quantitative results. For the former, we calculated metabolic maps of Cho and NAA using the freely available reconstruction program csx (Linux version), obtained from the homepage of the Kennedy Krieger Institute (Baltimore, Md). The magnitude of spectra was calculated, the position of NAA was set to 2.02 ppm, and a susceptibility correction was applied. The peak areas for Cho and NAA were calculated by integration over frequency ranges of 3.34–3.14 and 2.22–1.82 ppm, respectively. Smooth linear interpolation to a 256 × 256 matrix resulted in the metabolic maps. Cho and NAA images were used to calculate a map of Cho/NAA ratios. Segmentation of the tumor due to the metabolic changes related to the lesion in the Cho/NAA ratio map was performed by a method described previously.[20] Coregistration of conventional MR imaging (T2-weighted TSE and 3D MPRAGE), DTI data sets, and MRSI data in the form of a so-called MR imaging/MRSI hybrid data set[21] was performed at the planning workstation of a navigation system (VectorVision Sky; Brain LAB, Heimstetten, Germany) using a semiautomated coregistration (VV2 Planning 1.3; BrainLAB, Heimstetten, Germany).

For metabolite quantification from the MRSI data, we used the spectral fit program LCModel (version 6.1).[22] The spectra were analyzed as a linear combination of a set of reference basis spectra. For all spectroscopic data, we used the reference basis set for PRESS and TE of 135 ms. Our method for quantification of metabolite concentrations is similar to that published previously.[23,24] Molar metabolite concentrations out of the in vivo MRSI data were calculated on a workstation (Solaris SPARC; Sun Microsystems, Santa Clara, Calif) using a calibrated LCModel program. All spectral fits were performed in an analysis window from 1.8–4.0 ppm. Spectra with an SNR < 2 and a full width at half-maximum > 0.075 ppm were not included in the statistical analysis. In addition, metabolites with SD > 20%, as given by LCModel, were not included in the statistical analysis.

Statistical Analysis

Data were analyzed using statistical software (SPSS, version 12; SPSS, Chicago, Ill). For comparisons of results, 2-sided paired and unpaired *t* tests were used, with significance indicated by $P < .05$. To correlate the DTI (FA and MD) and fiber (FpV) parameters among themselves and with the 3 MRSI parameters (concentration of NAA and Cho, and Cho/NAA) we determined Pearson correlation coefficients (R) and P values for the test of significance. Interpretation of the correlation coefficients was made considering the specifications for interpretation of correlation coefficients given by Zou et al.[25]

Results

DTI and high spatial resolution MRSI data of suitable quality were obtained from both hemispheres for all patients. Analysis of data, including fiber tracking of the pyramidal tract, segmentation of pathologic metabolite changes in the Cho/NAA-ratio image, and coregistration of these results, were successfully performed in all cases. Overviews of the results obtained from the different aspects of data analysis for a patient having no sensorimotor deficits (patient 17 in Table 1) and a patient with hypesthesia in his right arm (patient 14 in Table 1) are presented in Figs 1 and 2, respectively.

Figs 1*B* and 2*B* show 3D reconstructions of the pyramidal tract on the ipsilateral (*blue*) and contralateral (*magenta*) side of the lesions. Figs 1*A*, -*C*, and 2*A*, -*C* demonstrate the coregistration of the T2-weighted TSE images and the segmented metabolic maps using software of the neuronavigation system. The profile of the pyramidal tracts (*blue and magenta line*) and the tumor (*yellow* or *green line*) are also depicted on these figures. No overlap of the ipsilateral pyramidal tract and the segmented metabolic map is indicated in the patient without sensorimotor deficits (Fig 1*B*). However, for the patient with hypesthesia of the right arm, the pyramidal tract extends into the segmented metabolic map. Overlapping pyramidal tract and segmented Cho/NAA maps were found in 5 of 8 patients (patients 1, 3, 12, 14, and 18) having sensorimotor deficits but in none of the other group. Spectra fitted by LCModel for a voxel position at the contralateral (*voxel 1* in Figs 1*C* and 2*C*) and ipsilateral (*voxel 2* in Figs 1*C* and 2*C*) pyramidal tract are given in Figs 1*D*, -*E*, and 2*D*, -*E*, respectively. Only in patients 1 and 18 were the ipsilateral pyramidal tracts located in hyperintense WM, identified on T2-weighted TSE and FLAIR images by a neuroradiologist as peritumoral edema. The pyramidal tracts of all other patients were located in the normal-appearing WM.

The DTI and fiber parameters for the ipsilateral and contralateral pyramidal tracts were calculated for the whole fiber bundle as well as for those 5 DTI sections that were on the same position as the MRSI section. The thickness of the 5 DTI sections was 9.5 mm overall and that of the MRSI section was 10 mm. However, in view of section warp and variability in section thickness, this difference is insignificant. For the whole pyramidal tract, we found, for the ipsilateral side, FpV = 8.6 ± 1.4 (mean ± SD), FA = 0.50 ± 0.03, and MD = 0.781 ± 0.091 × 10^{-3} mm^2/s and, for the contralateral side, FpV = 11.0 ± 1.1, FA = 0.53 ± 0.03, and MD = 0.745 ± 0.073 ×

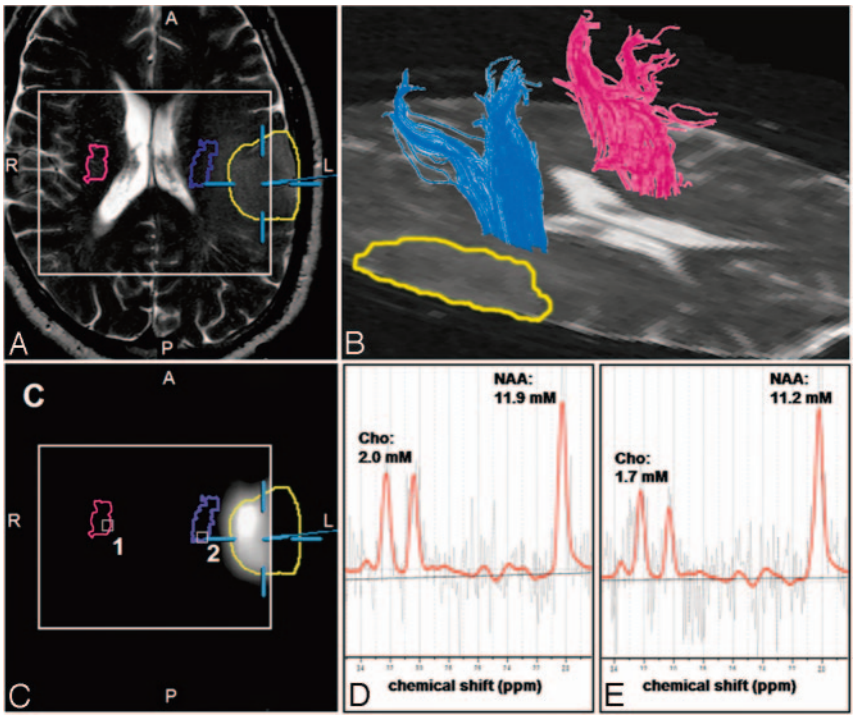

Fig 1. Results of the fiber-tracking procedure of the DTI data and the spectral analysis of the MRSI data for a patient having no sensorimotor deficits (patient 17 in Table 1). Screenshot from the planning workstation of a navigation system of an axial T2-weighted MR imaging (*A*) coregistered with a segmented metabolic Cho/NAA map (*C*). Overlaid on these images are the cross sections of the ipsilateral (*blue*) and contralateral (*magenta*) pyramidal tracts, the tumor segmented manually by a neurosurgeron (*yellow*), and the VOI (PRESS-box) of the MRSI experiment (*white rectangle*).

B, a 3D reconstruction of the ipsilateral (*blue*) and contralateral (*magenta*) pyramidal tracts depicted on the axial sections of the DTI dataset measured with a b-value = 0 s/mm^2. LCModel fits (*red line*) of the MRSI data of voxel position 1 (*D*) and 2 (*E*) as depicted in *C* as *white squares*. Overlaid on these images are the molar concentrations for Cho, Cr, and NAA calculated by LCModel.

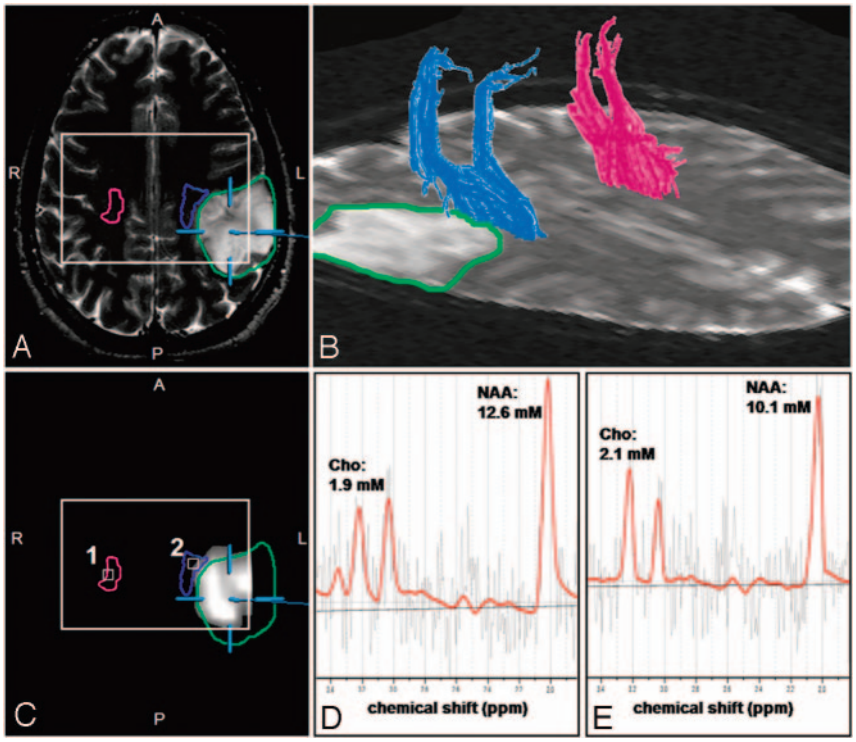

Fig 2. Results of the fiber-tracking procedure of the DTI data and the spectral analysis of the MRSI data for a patient with a hypesthesia in right arm (patient 14 in Table 1). Screenshot from the planning workstation of a navigation system of an axial T2-weighted MR imaging (*A*) coregistred with a segmented metabolic Cho/NAA map (*C*). Overlaid on these images are the cross sections of the ipsilateral (*blue*) and contralateral (*magenta*) pyramidal tracts, the tumor segmented manually by a neurosurgeon (*green*), and the PRESS-box of the MRSI experiment (*white rectangle*).

B, a 3D reconstruction of the ipsilateral (*blue*) and contralateral (*magenta*) pyramidal tracts depicted on the axial sections of the DTI dataset measured with a b-value = 0 s/mm^2. LCModel fits (*red line*) of the MRSI data of voxel positions 1 (*D*) and 2 (*E*) as depicted in *C* as *white squares*. Overlaid on these images are the molar concentrations for Cho, Cr, and NAA calculated by LCModel.

10^{-3} mm^2/s. Two-sided paired *t* tests revealed significant differences between ipsilateral and contralateral pyramidal tracts for FpV and FA, but not for MD (Fig 3).

For the DTI and fiber parameters averaged over the 5 DTI sections, which are correlated with the MRSI section ("pyramidal tract section"), we found, on the ipsilateral side, FpV = 8.0 ± 2.4, FA = 0.50 ± 0.04, and MD = 0.786 ± 0.076 × 10^{-3} mm^2/s and, for the contralateral side, FpV = 10.1 ± 2.9, FA = 0.56 ± 0.04, and MD = 0.724 ± 0.043 × 10^{-3} mm^2/s. Two-sided paired *t* tests revealed significant differences between the ipsilateral and contralateral sections of the pyramidal tracts for FpV, FA, and MD (Fig 4*A*–*C*).

Metabolic concentrations for NAA and Cho, and ratios of Cho/NAA were calculated for all voxel positions located in the pyramidal tract and averaged subsequently for the ipsilateral and contralateral fiber structure. To limit partial volume effects at least 75% of a voxels have to be located in the region of interest to be accepted for evaluation. Examples for several ipsilateral and contralateral voxel positions are marked as *small white squares* in Figs 1*C* and 2*C*. Concentrations were

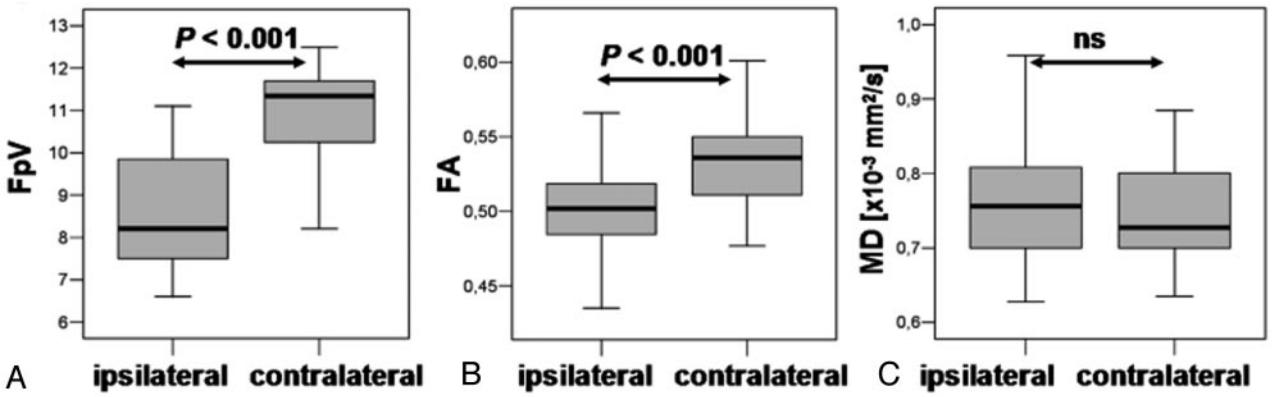

Fig 3. Shown are boxplots of FpV, FA, and MD values of the whole ipsilateral and contralateral pyramidal tracts (*A*, *B*, and *C*, respectively). The horizontal lines are the medians, and the ends of the boxes are the lower and upper quartiles (25th and 75th percentiles). MD values are expressed in units $\times 10^{-3}$ mm^2/s. The error bars depict the SD. Overlaid are the *P* values calculated from a 2-sided paired *t* test (ns = not significant).

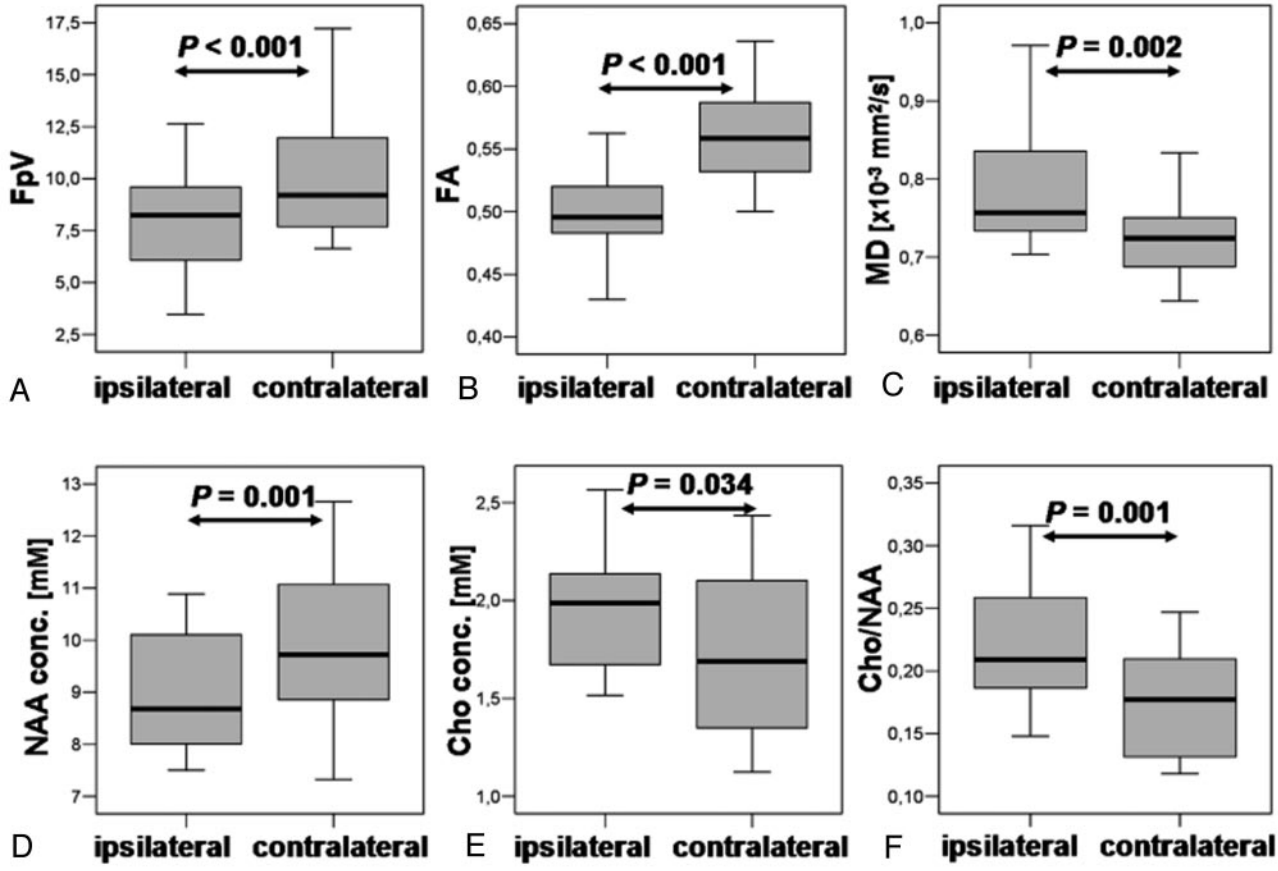

Fig 4. Shown are boxplots of FpV, FA, and MD values for the section of the ipsilateral and contralateral pyramidal tracts (*A*, *B*, and *C*, respectively) corresponding with the MRSI section, respectively. Boxplots of molar concentrations of NAA, Cho, and the Cho/NAA ratio averaged over voxel positions located at the ipsilateral and contralateral pyramidal tract cross sections (*D*, *E*, and *F*, respectively). MD values are expressed in units $\times 10^{-3}$ mm^2/s. NAA and Cho values are are expressed in millimoles per liter. Overlaid are the *P* values calculated from a 2-sided paired *t* test.

averaged and resulted in the following values for the ipsilateral pyramidal tract: NAA = 8.9 ± 1.2 mmol/L, Cho = 1.9 ± 0.3 mmol/L, and Cho/NAA = 0.22 ± 0.05, and for the contralateral pyramidal tract: NAA = 10.0 ± 1.4 mmol/L, Cho = 1.7 ± 0.4 mmol/L, and Cho/NAA = 0.17 ± 0.04. Two-sided paired *t* tests revealed significant differences between the ipsilateral and contralateral NAA and Cho concentrations as well as Cho/NAA ratios (Fig 4, *D–F*).

We found significant differences between patients having no sensorimotor deficits and patients with a paresis and/or sensory deficits on ipsilateral side for FA and MD (Fig 5) but not for other parameters (FpV, NAA, Cho, and Cho/NAA) and not for the contralateral side.

Table 2 shows a summary of *P* values for 2-sided paired *t* tests between ipsilateral and contralateral DTI and fiber parameters, and metabolic concentrations for subgroups of patients with and without sensorimotor deficits. For both subgroups, we found significant differences for FpV and FA for

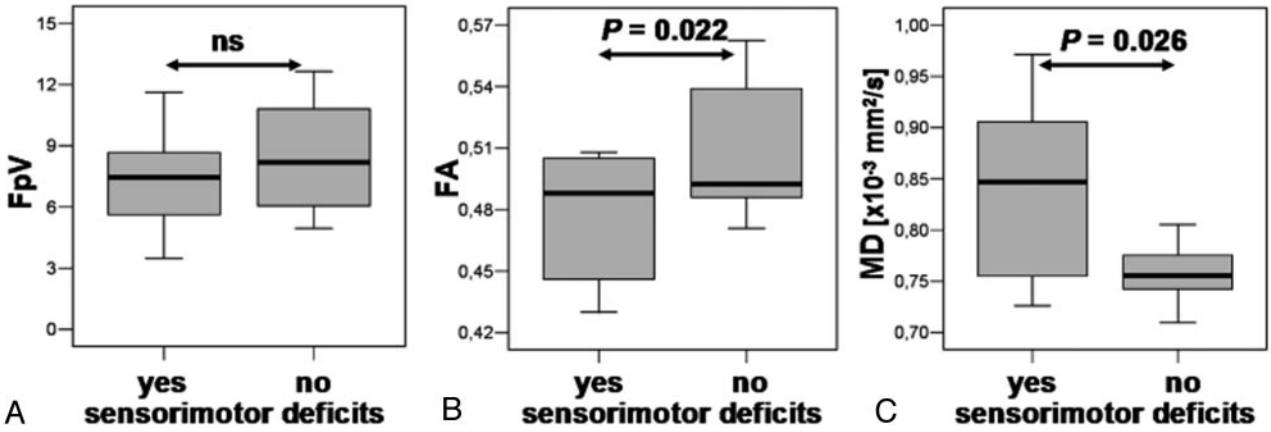

Fig 5. Boxplots of FpV, FA, and MD values of the section of the ipsilateral pyramidal tracts corresponding with the MRSI section for subgroups of patients without sensorimotor deficits, "no," and patients with sensorimotor deficits, "yes" (*A*, *B*, and *C*, respectively). MD values are expressed in units $\times 10^{-3}$ mm^2/s. Overlaid are the *P* values calculated from a 2-sided unpaired *t* test (ns = not significant).

Table 2: *P* values for *t* tests between ipsilateral and contralateral parameters and for subgroups of patients

Sensorimotor Deficits	Pyramidal Tract Total			Pyramidal Tract Section			MRSI		
	FpV	FA	MD	FpV	FA	MD	NAA	Cho	Cho/NAA
Yes (n = 8)	.002	<.001	.04	.024	<.001	.003	.011	.002	.001
No (n = 12)	<.001	<.001	NS	<.001	.009	NS	.033	NS	.047

Note:—FpV indicates fibers per voxel; FA, fractional anisotropy; MD, mean diffusivity; NS, nonsignificant. Statistical significance indicated by $P < .05$ using 2-sided paired *t* tests.

the whole pyramidal tract as well as for the section of the pyramidal tract (5 sections of the DTI dataset) with the shortest distance to the lesion and located at the MRSI section. MD showed significant differences between ipsilateral and contralateral pyramidal tract only for the subgroup of patients with sensorimotor deficits. Similar results were found for NAA and Cho/NAA by a *t* test that revealed significant differences between ipsilateral and contralateral voxel positions at the pyramidal tracts for both subgroups. For Cho, we found significant differences only in the subgroup of sensorimotor impaired patients.

Pearson correlation between FA and FpV revealed a strongly positive correlation for the contralateral side in patients with ($R = 0.826$, $P = .001$) and without ($R = 0.652$, $P = .002$) sensorimotor deficits, but not for the ipsilateral side. Only on the ipsilateral side, however, did we find a strongly negative correlation between FA and MD for patients with sensorimotor deficits ($R = -0.710$, $P = .024$) and no association for patients having no deficits ($R = 0.078$, ns). All other correlation analyses were found to be not significant, including correlations between DTI and fiber parameters and MRSI parameters.

Discussion

DTI and fiber tracking are methods to detect WM fiber tracts according to the anisotropy of water diffusion. ^{1}H-MRSI is a noninvasive tool for investigating the spatial distribution of metabolic changes in brain lesions. These MR imaging techniques have the potential to overcome a well-known insufficiency of standard MR imaging: the underestimation of impairment of WM fiber structures as a result of brain tumors.

Several studies have shown that fiber tracts in the vicinity of brain tumors might be displaced, disrupted, or invaded by the tumor.[5-7,26] However, all studies used only a qualitative approach to visually assess changes in the reconstructed fiber bundles. Two recent publications went a step further and used 3D reconstruction of fiber tracts to guide manually the selection of ROIs for quantitative analysis. A study by Schonberg et al[9] showed that along fiber systems that are displaced and compressed as a result of brain tumors, the diffusivity increases parallel and decreases perpendicular to the fibers. This leads to an overall increase of FA and to the conclusion that this may reflect the compression of the fiber bundle. Roberts et al[8] established a so-called fiber attenuation index (FDi) as measure of the number of fiber paths traversing a manually defined ROI to encompass corticospinal and corticopontine fibers. The authors noted that the FDi (as well as the FpV in our study) is not able to assess the real (absolute) number of fibers; rather, it gives a semiquantitative parameter that depends on imaging parameters (eg, spatial resolution) and postprocessing (eg, tracking thresholds).

Unlike the FDi, which is calculated from a 2-dimensional ROI, we determined diffusivity (ie, FA and MD) and fiber parameters (ie, FpV) averaged over a 3D VOI (that is, the whole as well as a section of the pyramidal tracts, which were defined using a fiber-tracking algorithm for semiautomatic segmentation of the VOI).

Our FA and MD values for the pyramidal tract section on the contralateral side agree with the data of Cosottini et al[27] for control subjects (FA = 0.585 and MD = 0.697×10^{-3} mm^2/s). However, FA values reported by 2 other studies for contralateral WM in patients ranges from 0.459[28] to 0.65.[8] For the ipsilateral side, our MD values correspond with those reported by Provenzale et al[28] for normal-appearing WM adjacent to hyperintense WM (0.723×10^{-3} mm^2/s), but for FA we found a higher value compared with this study (FA = 0.375) and with that of Roberts et al[8] (FA = 0.40). The differences between the values could be explained by different size of the

VOIs in our study and ROIs in the above-mentioned studies. We found significant differences for FA and MD on the ipsilateral side between the subgroups of patients with and without sensorimotor deficits. These differences are thought to reflect preoperative deficits. The different ranges of the MD values for the 2 subgroups were unexpected, an explanation for this fact will be provided below.

Between FA and FpV for the section of the pyramidal tract, we obtained a significant correlation only on the contralateral side for all 20 patients. Roberts et al[8] found a strong positive correlation ($R = 0.81$) between FA and FDi for a sample of values consisting of both peritumoral and contralateral WM, but they calculated no correlations for ipsilateral and contralateral ROIs separately. Between FA and MD, we found a strong negative correlation on the ipsilateral side for patients with sensorimotor deficits but not for patients without preoperative sensorimotor deficits. A study by Lu et al[29] showed a weak correlation ($R = -0.44$) between FA and MD in peritumoral edema of gliomas, defined as a hyperintense area on T2-weighted MR images. Price et al[30] and Wieshmann et al[31] showed that the isotropic component of the diffusion tensor has a limited range and the anisotropic component has a marked range in healthy control subjects. Unfortunately, none of the studies mentioned performed correlation analyses between the components for either the control subjects or the contralateral normal-appearing WM.

In 18 of 20 patients of this study, the ipsilateral pyramidal tract was located outside of the peritumoral edema visible on conventional MR images (ie, in peritumoral normal-appearing WM). However, the differences between ipsilateral and contralateral DTI and fiber parameters as well as the correlations between FA and FpV, and between FA and MD, respectively, indicates an edematous change not detectable by conventional T2-weighted MR imaging. Further, correlation between FA and MD for patients with sensorimotor deficits and the differences in the range of MD between the subgroups can be interpreted as a distinct increase of extracellular water.

The molar concentrations for Cho and NAA and the values for Cho/NAA ratio on the ipsilateral as well as on the contralateral side agree with findings in healthy volunteers from other studies.[5,32-35] The means and ranges of values calculated from the results of 5 studies also using a phantom replacement technique for quantification are: Cho, 1.7 mmol/L (1.5–1.9 mmol/L), NAA, 9.4 mmol/L (8.0–10.7 mmol/L), and Cho/NAA, 0.18 (0.14–0.26). However, we found significant differences between ipsilateral and contralateral sides for all 3 metabolic parameters in all 20 patients, but no significant differences between subgroups. These findings support the results obtained from DTI and fiber tracking. An increase of extracellular water causes a dilution and hence leads to a decrease of NAA. Also this process results in a higher molecular mobility of the choline-containing compounds and hence to an increase of the T2 relaxation time and, subsequently, an increase in "MR-visible" Cho concentration.[36,37]

The differences in spatial resolution of the DTI (1.9 mm^3 isotropic voxels) and the MRSI ($5 \times 5 \times 10$ mm^3) is a limitation of our study. Hence, partial volume effects occurred for our MRSI findings despite increasing the spatial resolution in MRSI to the limit to obtain spectra with sufficient SNR at 1.5T and in acquisition times acceptable for patients with glioma. The DTI method used in our study is limited by the fact that we used no parallel imaging technique (spin-echo acquisition and sensitivity encoding or generalized autocalibrating partially parallel acquisition), which would allow reduction in susceptibility and motion artifacts. However, because of the reduction in SNR involved with this technique and to obtain MRSI data with higher spatial resolution, it would be necessary to go to higher magnetic field strengths (3T or more).[38] In this study, we used manual placement of the ROI, which is always afflicted with the possibility of anatomic or functional mismatch. Therefore, the possibility exists that other pathways were reconstructed. By our protocol of placing 2 ROIs (in the sensorimotor cortex and in the posterior limb of the internal capsule), which was done by a neuroanatomically experienced neuroradiologist, we tried to keep this uncertainty as low as possible. Another limitation of our study was the relatively small number of patients, especially for the subgroups of patients with sensorimotor deficits ($n = 8$).

Conclusion

DTI in combination with quantitative fiber tracking adds to a better characterization of changes of the pyramidal tract adjacent to brain tumors. We detected significant differences of metabolic changes in these WM structures compared with contralateral normal-appearing WM using ^{1}H-MRSI with high spatial resolution at 1.5T. DTI and ^{1}H-MRSI can provide information on changes in WM structures, which are not detectable by conventional MR imaging. Quantitative DTI is able to show significant differences in diffusivity of the pyramidal tract in patients with sensorimotor deficits in relation to patients without them. The additional use of ^{1}H-MRSI may be helpful to discern whether these diffusivity changes in fiber tracts are caused by tumor infiltration or peritumoral edema.

References

1. Mori S, Crain BJ, Chacko VP, et al. **Three-dimensional tracking of axonal projections in the brain by magnetic resonance imaging.** *Ann Neurol* 1999;45:265–69
2. Jones DK, Simmons A, Williams SC, et al. **Non-invasive assessment of axonal fiber connectivity in the human brain via diffusion tensor MRI.** *Magn Reson Med* 1999;42:37–41
3. Le Bihan D, Mangin JF, Poupon C, et al. **Diffusion tensor imaging: concepts and applications.** *J Magn Reson Imaging* 2001;13:534–46
4. Mori S, Kaufmann WE, Davatzikos C, et al. **Imaging cortical association tracts in the human brain using diffusion-tensor-based axonal tracking.** *Magn Reson Med* 2002;47:215–23
5. Nimsky C, Ganslandt O, Hastreiter P, et al. **Intraoperative diffusion-tensor MR imaging: shifting of white matter tracts during neurosurgical procedures–initial experience.** *Radiology* 2005;234:218–25
6. Clark CA, Barrick TR, Murphy MM, et al. **White matter fiber tracking in patients with space-occupying lesions of the brain: a new technique for neurosurgical planning?** *Neuroimage* 2003;20:1601–08
7. Yamada K, Kizu O, Mori S, et al. **Brain fiber tracking with clinically feasible diffusion-tensor MR imaging: initial experience.** *Radiology* 2003;227:295–301
8. Roberts TP, Liu F, Kassner A, et al. **Fiber density index correlates with reduced fractional anisotropy in white matter of patients with glioblastoma.** *AJNR Am J Neuroradiol* 2005;26:2183–86
9. Schonberg T, Pianka P, Hendler T, et al. **Characterization of displaced white matter by brain tumors using combined DTI and fMRI.** *Neuroimage* 2006
10. Berman JI, Mukherjee P, Partridge SC, et al. **Quantitative diffusion tensor MRI fiber tractography of sensorimotor white matter development in premature infants.** *Neuroimage* 2005;27:862–71
11. Majos C, Alonso J, Aguilera C, et al. **Adult primitive neuroectodermal tumor: proton MR spectroscopic findings with possible application for differential diagnosis.** *Radiology* 2002;225:556–66
12. Negendank WG, Sauter R, Brown TR, et al. **Proton magnetic resonance spectroscopy in patients with glial tumors: a multicenter study.** *J Neurosurg* 1996;84:449–58

13. Michaelis T, Merboldt KD, Bruhn H, et al. **Absolute concentrations of metabolites in the adult human brain in vivo: quantification of localized proton MR spectra.** *Radiology* 1993;187:219–27
14. Urenjak J, Williams SR, Gadian DG, et al. **Proton nuclear magnetic resonance spectroscopy unambiguously identifies different neural cell types.** *J Neurosci* 1993;13:981–89
15. Horska A, Calhoun VD, Bradshaw DH, et al. **Rapid method for correction of CSF partial volume in quantitative proton MR spectroscopic imaging.** *Magn Reson Med* 2002;48:555–58
16. Jiang H, van Zijl PC, Kim J, et al. **DtiStudio: resource program for diffusion tensor computation and fiber bundle tracking.** *Comput Methods Programs Biomed* 2006;81:106–16
17. Pierpaoli C, Basser PJ. **Toward a quantitative assessment of diffusion anisotropy.** *Magn Reson Med* 1996;36:893–906
18. Xue R, van Zijl PC, Crain BJ, et al. **In vivo three-dimensional reconstruction of rat brain axonal projections by diffusion tensor imaging.** *Magn Reson Med* 1999;42:1123–27
19. Stadlbauer A, Gruber S, Nimsky C, et al. **Gliomas: histopathologic evaluation of changes in directionality and magnitude of water diffusion at diffusion-tensor MR imaging.** *Radiology* 2006;240:803–10
20. Stadlbauer A, Moser E, Gruber S, et al. **Improved delineation of brain tumors: an automated method for segmentation based on pathologic changes of 1H-MRSI metabolites in gliomas.** *Neuroimage* 2004;23:454–61
21. Stadlbauer A, Moser E, Gruber S, et al. **Integration of biochemical images of a tumor into frameless stereotaxy achieved using a magnetic resonance imaging/magnetic resonance spectroscopy hybrid data set.** *J Neurosurg* 2004;101:287–94
22. Provencher SW. **Estimation of metabolite concentrations from localized in vivo proton NMR spectra.** *Magn Reson Med* 1993;30:672–79
23. Stadlbauer A, Gruber S, Nimsky C, et al. **Preoperative grading of gliomas by using metabolite quantification with high-spatial-resolution proton MR spectroscopic imaging.** *Radiology* 2006;238:958–69
24. McLean MA, Woermann FG, Barker GJ, et al. **Quantitative analysis of short echo time (1)H-MRSI of cerebral gray and white matter.** *Magn Reson Med* 2000;44:401–11
25. Zou KH, Tuncali K, Silverman SG. **Correlation and simple linear regression.** *Radiology* 2003;227:617–22
26. Mori S, Frederiksen K, van Zijl PC, et al. **Brain white matter anatomy of tumor patients evaluated with diffusion tensor imaging.** *Ann Neurol* 2002;51:377–80
27. Cosottini M, Giannelli M, Siciliano G, et al. **Diffusion-tensor MR imaging of corticospinal tract in amyotrophic lateral sclerosis and progressive muscular atrophy.** *Radiology* 2005;237:258–64
28. Provenzale JM, McGraw P, Mhatre P, et al. **Peritumoral brain regions in gliomas and meningiomas: investigation with isotropic diffusion-weighted MR imaging and diffusion-tensor MR imaging.** *Radiology* 2004;232:451–60
29. Lu S, Ahn D, Johnson G, et al. **Diffusion-tensor MR imaging of intracranial neoplasia and associated peritumoral edema: introduction of the tumor infiltration index.** *Radiology* 2004;232:221–28
30. Price SJ, Pena A, Burnet NG, et al. **Tissue signature characterisation of diffusion tensor abnormalities in cerebral gliomas.** *Eur Radiol* 2004;14:1909–17
31. Wieshmann UC, Clark CA, Symms MR, et al. **Reduced anisotropy of water diffusion in structural cerebral abnormalities demonstrated with diffusion tensor imaging.** *Magn Reson Imaging* 1999;17:1269–74
32. Soher BJ, Hurd RE, Sailasuta N, et al. **Quantitation of automated single-voxel proton MRS using cerebral water as an internal reference.** *Magn Reson Med* 1996;36:335–39
33. Keevil SF, Barbiroli B, Brooks JC, et al. **Absolute metabolite quantification by in vivo NMR spectroscopy: II. A multicentre trial of protocols for in vivo localised proton studies of human brain.** *Magn Reson Imaging* 1998;16:1093–106
34. Pouwels PJ, Brockmann K, Kruse B, et al. **Regional age dependence of human brain metabolites from infancy to adulthood as detected by quantitative localized proton MRS.** *Pediatr Res* 1999;46:474–85
35. Helms G. **A precise and user-independent quantification technique for regional comparison of single volume proton MR spectroscopy of the human brain.** *NMR Biomed* 2000;13:398–406
36. Kamada K, Houkin K, Hida K, et al. **Localized proton spectroscopy of focal brain pathology in humans: significant effects of edema on spin-spin relaxation time.** *Magn Reson Med* 1994;31:537–40
37. Kamada K, Houkin K, Iwasaki Y, et al. **In vivo proton magnetic resonance spectroscopy for metabolic changes of human brain edema.** *Neurol Med Chir (Tokyo)* 1994;34:676–81
38. Gruber S, Mlynarik V, Moser E. **High-resolution 3D proton spectroscopic imaging of the human brain at 3 T: SNR issues and application for anatomy-matched voxel sizes.** *Magn Reson Med* 2003;49:299–306